Combining Protein Phase Separation and Bio-orthogonal Linking to Coimmobilize Enzymes for Cascade Biocatalysis

Wu, Shujiao; Luo, Lingling; Luo, Houtian; Qiao, Li; Chen, Haomin; Li, Mijun; Pei, Xiaolin; Xie, Tian; Wang, Anming; Sheldon, Roger A.

DOI
10.1002/smll.202404018

Publication date
2024

Document Version
Final published version

Published in
Small

Citation (APA)
Wu, S., Luo, L., Luo, H., Qiao, L., Chen, H., Li, M., Pei, X., Xie, T., Wang, A., & Sheldon, R. A. (2024). Combining Protein Phase Separation and Bio-orthogonal Linking to Coimmobilize Enzymes for Cascade Biocatalysis. *Small*, *20*(51), Article 2404018. https://doi.org/10.1002/smll.202404018

RESEARCH ARTICLE

NANO · MICRO small
www.small-journal.com

Combining Protein Phase Separation and Bio-orthogonal Linking to Coimmobilize Enzymes for Cascade Biocatalysis

Shujiao Wu, Lingling Luo, Houtian Luo, Li Qiao, Haomin Chen, Mijun Li, Xiaolin Pei, Tian Xie, Anming Wang,* and Roger A. Sheldon**

The designed and ordered co-immobilization of multiple enzymes for vectorial biocatalysis is challenging. Here, a combination of protein phase separation and bioorthogonal linking is used to generate a zeolitic imidazole framework (ZIF-8) containing co-immobilized enzymes. Zn^{2+} ions induce the clustering of minimal protein modules, such as 6-His tag, proline-rich motif (PRM) and SRC homology 3 (SH3) domains, and allow for phase separation of the coupled aldoketoreductase (AKR) and alcohol dehydrogenase (ADH) at low concentrations. This is achieved by fusing SpyCatcher and PRM-SH3-6His peptide fragments to the C and N termini of AKR, respectively, and the SpyTag to ADH. Addition of 2-methylimidazole results in droplet formation and enables in situ spatial embedding the recombinant AKR and ADH to generate the cascade biocalysis system encapsulated in ZIF-8 (AAE@ZIF). In synthesizing (S)-1-(2-chlorophenyl) ethanol, ater 6 cycles, the yield can still reach 91%, with 99.99% enantiomeric excess (ee) value for each cycle. However, the yield could only reach 72.9% when traditionally encapsulated AKR and ADH in ZIF-8 are used. Thus, this work demonstrates that a combination of protein phase separation and bio-orthogonal linking enables the in situ creation of a stable and spatially organized bi-enzyme system with enhanced channeling effects in ZIF-8.

1. Introduction

Multienzyme cascade biocatalysis is used to produce a wide range of fine chemicals and pharmaceuticals by combining multiple biocatalytic steps in one pot, offering a time-saving and lower-cost alternative to separate single-step reactions.[1,2] In multienzyme systems, intermediates can be rapidly converted to the final product by downstream enzymes.[2] Compared to randomly dispersed enzymes,[3–6] clustering enzymes together in cascades streamlines metabolic flow to desired products by promoting the transfer of intermediates, hindering their leakage, and reducing side effects caused by toxic intermediates.[7] This translates to shorter cycle times, smaller unit operations, reduced reactor size, and increased space-time yields,[8] resulting in reduced costs, less waste generation and more sustainable processes.[9]

Using cascade biocatalysis in vitro to synthesize the antiviral HIV drug, islatravir[2] required less than half the number of steps compared to the previously reported method and an overall yield of more than 50%. Thus, the use of multi-enzyme cascade biocatalysis, combined with the benefits of enzyme immobilization, has led to the development of strategies for co-localizing multiple enzymes on nanosupports and creating multienzyme nanocubes.[1,10] However, their widespread application is limited by two disadvantages: i) the use of covalent linking using glutaraldehyde or epoxy groups as a cross-linking agent[11] results in random and disordered localization of enzymes and ii) expensive purified enzymes are generally used.

Metal-organic frameworks (MOFs) are microporous crystalline organic-inorganic hybrid materials constructed from metal ions and organic linkers. Zn^{2+} ion is one of the components used to produce zeolitic imidazolate framework-8 (ZIF-8), a member of the MOF family, formed by coordination between Zn^{2+}

S. Wu, L. Luo, H. Luo, M. Li, T. Xie
School of Pharmacy
Hangzhou Normal University, China
Hangzhou, Zhejiang 311121, China
E-mail: xbs@hznu.edu.cn

L. Qiao, H. Chen, X. Pei, A. Wang
College of Materials Chemistry and Chemical Engineering
Hangzhou Normal University
Hangzhou, Zhejiang 311121, China
E-mail: waming@hznu.edu.cn

R. A. Sheldon
Molecular Sciences Institute
School of Chemistry
University of the Witwatersrand
Johannesburg PO Wits. 2050, South Africa
E-mail: roger.sheldon@wits.ac.za

R. A. Sheldon
Department of Biotechnology
Section BOC
Delft University of Technology
van der Maasweg 9, Delft 2629 HZ, The Netherlands

The ORCID identification number(s) for the author(s) of this article can be found under https://doi.org/10.1002/smll.202404018

DOI: 10.1002/smll.202404018

and 2-methylimidazole.[12] MOFs have high surface areas and excellent porosity coupled with, extraordinary multifunctionality and relatively high stability, Based on their unique physical and chemical properties and inexpensive starting materials, MOFs are potentially viable candidates for enzyme immobilization platforms[13] with potential for industrial applications.[14,15] The methods for preparing an enzyme-MOFs can be divided into two categories, one is postsynthesis,[16] and the other is in situ encapsulation.[5] Compared to the former, in situ encapsulation means that the nucleation and crystallization of MOFs and the encapsulation of enzymes are carried out simultaneously. Here, the ZIFs family of MOFs (especially ZIF-8), which are synthesized under milder conditions, have been the preferred choice for experimental in situ synthesis as nanocarriers for immobilized enzymes. In forming ZIF-8, Zn^{2+} is so biocompatible that the in situ immobilized enzymes can retain high enzyme activity. This method has been used to load enzymes/proteins into ZIF pores with enhanced activity, recyclability, and solvent tolerance.[17,18] Moreover, efficient biocatalytic cascades are achieved by encapsulating two or three enzymes or enzyme/cofactor components in zeolite imidazoline framework-8 (ZIF-8).[19,20]

In addition to the usage in facilely producing zeolitic imidazolate framework-8 (ZIF-8),[21] biocompatible Zn^{2+} can accelerate the protein liquid–liquid phase separation (LLPS) through interactions with specific amino acids in minimal scaffolding modules such as 6Histidine-Tag (6His).[22] Protein liquid–liquid phase separation (LLPS) is an efficient way of condensing, enriching, and collecting target enzymes in cell lysate supernatant.[7,23] Most of all, protein phase separation rapidly induces the formation of protective MOF coatings under physiological conditions by concentrating the framework building blocks and facilitating crystallization around the biomacromolecules. It often occurs through the formation and compartmentalization of multienzyme complexes with a fixed stoichiometry and geometry.[24–26] The SH3/PRM system fused to target proteins is an efficient tool to achieve such phase separation in vitro.[27,28] In this system, the SRC homology 3 (SH3) domain binds to proline-rich motifs (PRM) and can condense into liquid droplets above a saturation concentration.[29] This allows for a wide range of scaffolding variations and precise control of dynamic droplet behavior.[22,30,31] Typically, Zn^{2+} ions can accumulate these protein droplets via 6His-Tag[22] when imidazole groups of His interact with them, accelerating the formation of prenucleation clusters.[17]

As well known, it is feasible and viable to facilitate the cascade reaction by precisely controlling the localization and orientation of the enzymes through appropriate immobilization strategies.[32] In our previous work, we achieved precise and orderly multi-enzyme assembly using bioorthogonal click chemistry.[33] Improved catalytic efficiency was observed, compared to free enzyme preparations, when cell lysate supernatants were mixed. However, the use of non-canonical amino acids (ncAAs) can be somewhat toxic to cells. This drawback can be circumvented by using canonical amino acids (cAAs) for bioorthogonal linking.[34] In recent years, covalent o-peptide labeling technology has garnered significant research interest as a "molecular glue" with great affinity for protein partners. Several reaction pairs have been developed, including SpyTag and SpyCatcher, SnoopTag and SnoopCatcher, and SdyTag and SdyCatcher.[34] Such a reaction is genetically encodable, thus allowing us to program posttranslational modifications of proteins within the cell and extend the protein backbone. The SpyTag-SpyCatcher system is ideal for creating irreversible peptide–protein junctions that spontaneously form covalent isopeptide linkages under physiological conditions.[35] This occurs simply by mixing the corresponding crude cell extracts.[36]

Chiral alcohol structures are widely present in a large number of biologically active molecules and drug components, thus its production is important in pharmaceutical industrial applications.[37,38] Most asymmetric reductions of ketones are catalyzed by aldehyde ketone reductase (AKR), and the expensive nicotinamide cofactors nicotinamide adenine dinucleotide (NADH) or nicotinamide adenine dinucleotide phosphate (NADPH) acting as hydrogen donors is regenerated using alcohol dehydrogenase (ADH). Therefore, we can jointly use AKR and ADH in the cascade catalytic system, in which isopropanol and NADP+ are first catalyzed by ADH to obtain NADPH. Then obtained NADPH enters the active pocket of AKR to participate in the enzymatic asymmetric reduction of prochiral ketones to chiral alcohols.[38] Thus, enzymatic synthesis of L-clorprenaline and thiophene-benzimidazole intermediate, (S)−1-(2-chlorophenyl) ethanol,[37] was chosen as a model reaction to evaluate and verify the effect which results from in situ encapsulation of enzymes in ZIF-8.

Herein, we fused the protein modules 6His-PRM-SH3 and SpyCatcher dock to AKR at the N and C terminals, respectively, after fusing the SpyTag dock to ADH. Subsequently, the cell lysates containing the two recombinant enzymes were mixed. Zn^{2+} was dispersed into the mixture to form liquid protein condensates while bio-orthogonal coupling using SpyTag-SpyCatcher docks occurred. Dimethylimidazole was further added to the crude enzyme solution to generate ZIF-8 containing a spatial dual enzyme cascade system in situ (**Scheme 1**). The phase separation of liquid proteins was examined using CLSM and a microscope and the catalytic properties were investigated in the presence of $NADP^+$ during the synthesis of (S)−1-(2-chlorophenyl) ethanol.

2. Results and Discussions

2.1. Design, Preparation, and Characterization of Synthetic Biomolecular Condensates

We employed specific interactions between modular protein and receptor–peptide ligands to create controllable protein condensates. Modular proteins allow precise manipulation of scaffold properties that drive liquid–liquid phase separation (LLPS).[7,39] Among various multivalent modular domain/ligand systems that drive LLPS, we initially utilized the second SH3 domain from Nck (SH3), and its binding proline-rich motif (PRM) (Figure S1a, Supporting Information). The binding structures of SH3/PRM are well known.[40] 6His-tagged SH3 and PRM fusion protein (PRM-SH3-6His) can accelerate phase separation into liquid droplets in the presence of metal ions such as Co, Cu, and Zn, etc.[22] Zinc ions were selected for their biocompatibility and avoidance of heavy metal residues during the synthesis of drug intermediates.

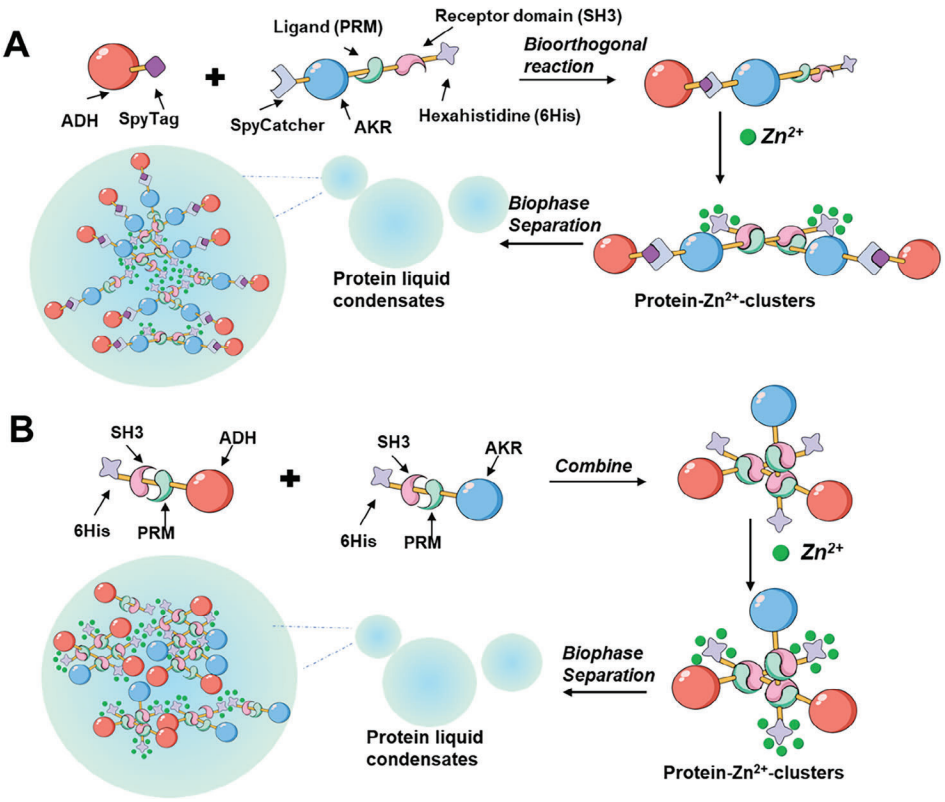

Scheme 1. Encapsulation of dual enzymes system in ZIF-8. A) Formation of sequential ADH/AKR system (SAAS) combining bioorthogonal ligation and protein phase separation. B) Formation of ADH/AKR system (AAS) using just protein phase separation.

In this work, the cascade reaction system of AKR and ADH was expected to efficiently convert ketones to chiral alcohols, with regeneration of NADPH from $NADP^+$. We used simple 6His-tagged SH3 and PRM domains (PRM-SH3-6His) that can be spontaneously phase-separated into droplets in the presence of Zn^{2+} We constructed AKR-PRM-SH3-6His and ADH-PRM-SH3-6His using a simple 6His-tagged SH3 and PRM (PRM-SH3-6His) and fused SpyCatcher domains to AKR, respectively (**Figure** 1A,C). Unfortunately, the fusion of a PRM-SH3-6His to the C-terminus of ADH greatly diminished its catalytic activity and also reduced protein expression. This may be a result from that ADH is a $NADP^+$-dependent short-chain reductase and its structure is fragile in folding and refolding besides a catalytic activity dependent on Mg^{2+}.[41] Attaching Spy/Cather to the C-terminus of ADH may lead to the loss of Mg^{2+} or hinder the catalytic reaction. Therefore, we had to just attach the corresponding domains to the N terminal of ADH (Figure 1A,D).

To examine and verify the phase behavior of combining 6His-SH3-PRM-ADH/AKR-PRM-SH3-6His (AAS) in vitro, we mixed them with a droplet formation buffer (5% polyethylene glycol 2000), the AAS protein immediately became cloudy, and turbid, and the turbidity (OD_{350}) grew from 0.143 ± 0.005 (2×10^{-6} M) to 1.255 ± 0.015 (60×10^{-6} M) with an increase in AAS protein concentration and the addition of Zn^{2+} in a manner dependent on metal concentration (**Figure** 2B and Table S5, Supporting Information). Droplet size also increases with protein concentration and Zn^{2+} concentration (Figure 2A). They can separate into droplets in the presence of Zn^{2+} (Figure 2C and Figure S4a, Supporting Information). The impact of Zn^{2+} concentrations on forming the liquid droplets for recombinant target protein was illustrated in Figure S2 (Supporting Information). The liquid droplet diameter also increased with the elevated proportion of cell lysis and shaking time (Figure S3, Supporting Information). As a result, PRM-SH3-6His fused proteins successfully underwent phase separation into liquid condensates upon the addition of Zn^{2+} (Figure 2) at lower protein concentrations.[25]

Dynamic droplet coalescence, a representative liquid-like property of protein liquid condensates, was also affirmed in all the formed protein condensates. When we fused GFP and mCherry proteins to target enzymes (Table S1, Supporting Information), they were also clearly enriched inside the droplets. Because the SH3 structural domain can bind to the PRM structural domain, many separate red droplets are formed by the intermolecular binding of mCherry-fused AKR-PRM-SH3-6His and green droplets are formed by the intermolecular binding of GFP-fused 6His-SH3-PRM-ADH. Co-localized yellow droplets demonstrate the red mCherry-fused AKR-PRM-SH3-6His merge with green GFP-fused 6His-SH3-PRM-ADH.[22,40] The "CFI" and "MFI" refer to the co-localized and total merged fluorescence intensity of GFP and mCherry, respectively (Figure 2F). The results show that during the formation of droplets, intramolecular and intermolecular binding of 6His-SH3-PRM-ADH and AKR-PRM-SH3-6His.

In addition, the diffusivity of proteins inside droplets was measured using fluorescence recovery after photobleaching (FRAP) analyses (Figure 2G). Proteins (100×10^{-6} M) and Zn^{2+}

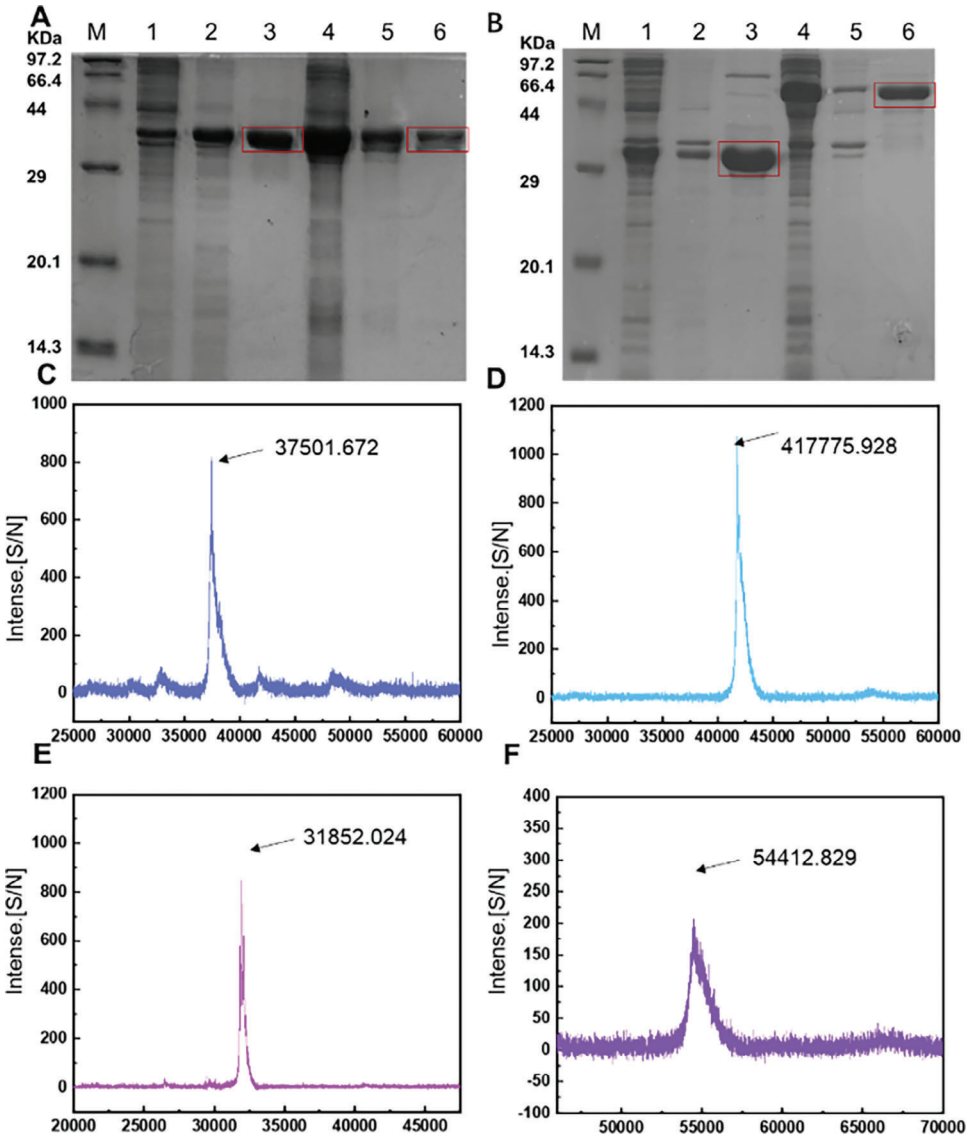

Figure 1. SDS-PAGE analysis of AKR-PRM-SH3-6His, 6His-SH3-PRM-ADH; SpyCatcher-AKR-PRM-SH3-6His, SpyTag-ADH: A) (M, Marker; Line 1, cell lysate supernatant of 6His-SH3-PRM-ADH; Line 2, insoluble in cell lysate of 6His-SH3-PRM-ADH; Line 3, purified 6His-SH3-PRM-ADH. Line 4, cell lysate supernatant of AKR-PRM-SH3-6His; Line 5, insoluble in cell lysate of AKR-PRM-SH3-6His; Line 6, purified AKR-PRM-SH3-6His. B) (M, Marker; Line 1, cell lysate supernatant of SpyTag-ADH; Line 2, insoluble in cell lysate of SpyTag-ADH; Line 3, purified SpyTag-ADH. Line 4, cell lysate supernatant of SpyCatcher-AKR-PRM-SH3-6His; Line 5, insoluble in cell lysate of SpyCatcher-AKR-PRM-SH3-6His; Line 6, purified SpyCatcher-AKR-PRM-SH3-6His. MALDI-TOF-MS analysis of AKR-PRM-SH3-6His, 6His-SH3-PRM-ADH; SpyCatcher-AKR-PRM-SH3-6His, SpyTag-ADH. (C, 6His-SH3-PRM-ADH; D, AKR-PRM-SH3-6His; E, SpyTag-ADH; F, SpyCatcher-AKR-PRM-SH3-6His.).

(20×10^{-6} M) were mixed and incubated for 60 min before FRAP. PRM-SH3-6His fused protein droplets exhibited clear fluorescence recovery from bleached areas, indicating a high mobile fraction for PRM-SH3-6His.[22]

2.2. Precise Alignment of Multiple Enzymes in Condensates through Bioorthogonal Coupling of Canonical Amino Acids

The ability to introduce various biomolecules into condensates is a key characteristic of protein condensates functioning as membrane-less organelles. In general, clients can be recruited into condensates by incorporating condensate-forming scaffold components into clients. If recruiting two target enzyme proteins for cascade biocatalysis, interacting motifs have to be utilized to achieve precise localization. In order to fully maintain the enzyme structure and activity, the motifs need to act as bioorthogonal binding pairs with previous and subsequent clients. The SpyCatcher-SpyTag motif, derived from the CnaB2 domain of Streptococcus pyogenes mucin FbaB, can form stable and specific amide bonds (isopeptide bonds), using ε-NH2 from Lys through bioorthogonal chemical modes, which serve as a foundation for constructing modular proteins. The CnaB2 domain consists of two parts: the immunoglobulin-like domain

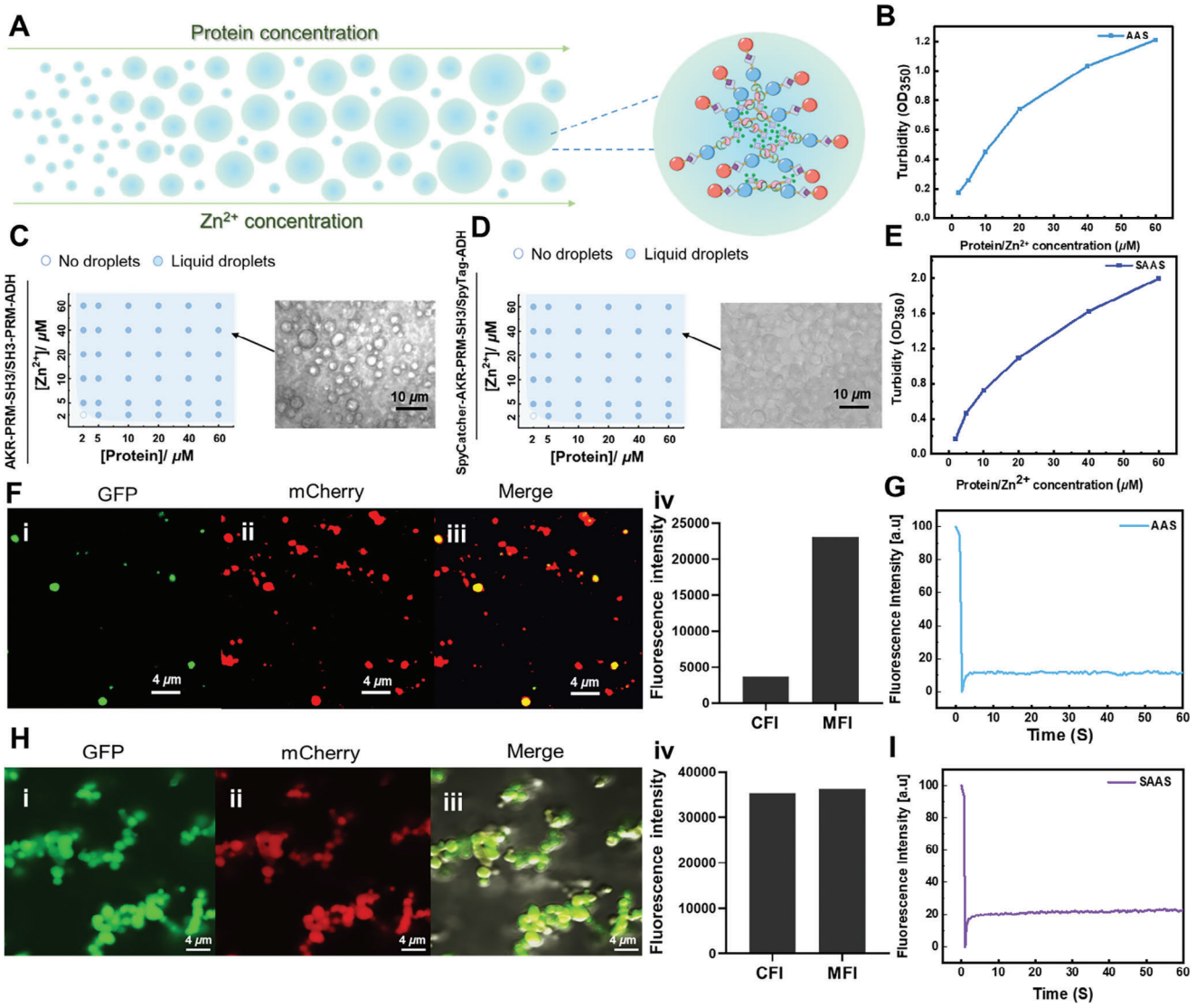

Figure 2. Formation and characterization of AKR/ADH condensates by phase separation. A) Fusion structural domain protein functionalized droplet size. B) Turbidity analysis of combining 6His-SH3-PRM-ADH/AKR-PRM-SH3-6His (AAS) protein concentrations and Zn^{2+} concentrations under droplet formation buffer (5% PEG2000). C) Phase diagram of AAS proteins as a function of Zn^{2+} and scaffold protein concentrations. Optical images of protein condensate at 60×10^{-6} M protein and 40×10^{-6} M Zn^{2+} (analysis after 18 h upon metal addition) are shown on the right. Scale bars: 10 μm. D) Phase diagram of combining SpyTag-ADH/SpyCatcher-AKR-PRM-SH3-6His (SAAS) proteins as a function of Zn^{2+} and scaffold protein concentrations. Optical images of protein condensate at 60×10^{-6} M protein and 40×10^{-6} M Zn^{2+} (analysis after 18 h upon metal addition) are shown on the right. Scale bars: 10 μm. E) Turbidity analysis of different SAAS protein concentrations and Zn^{2+} concentrations under droplet formation buffer (5% PEG2000). F) Confocal laser scanning microscope (CLSM) images of protein condensate at 30×10^{-6} M protein of the GFP-fused 6His-SH3-PRM-ADH and mCherry-fused AKR-PRM-SH3-6His and 20×10^{-6} M Zn^{2+} (analysis after 18 h upon metal addition). Excitation of the protein condensate AAS at 488 nm and monitoring the fluorescence of the GFP-fused 6His-SH3-PRM-ADH at 507 nm; excitation of the AAS at 588 nm and monitoring the fluorescence of the mCherry-fused AKR-PRM-SH3-6His at 610 nm. Scale bars: 40 μm. Histogram of AAS fluorescence intensity analysis. The "CFI" and "MFI" refer to the colocalized and total merged fluorescence intensity of GFP and mCherry, respectively. G) FRAP recovery profiles and images of AAS scaffold proteins inside condensates GFP-6His-SH3-PRM-ADH and mCherry-AKR-PRM-SH3-6His (analysis after 1 h upon metal addition). H) CLSM images of protein condensate at 30×10^{-6} M protein of the GFP-fused SpyTag-ADH and mCherry-fused SpyCatcher-AKR-PRM-SH3-6His and 20×10^{-6} M Zn^{2+} (analysis after 18 h upon metal addition). Excitation of the protein condensate at 488 nm and monitoring the fluorescence of the GFP-fused SpyTag-ADH at 507 nm; excitation of the protein condensate at 588 nm and monitoring the fluorescence of the mCherry-fused SpyCatcher-AKR-PRM-SH3-6His at 610 nm. Scale bars: 4 μm. Histogram of SAAS fluorescence intensity analysis. The "CFI" and "MFI" refer to the co-localized and total merged fluorescence intensity of GFP and mCherry, respectively (I) FRAP recovery profiles and images of SAAS scaffold proteins inside condensates (analysis after 1 h upon metal addition).

SpyCatcher, which is composed of 138 residues (15 KDa), and the short peptide SpyTag, which consists of 13 residues[34] (Figure S1b, Supporting Information). We incorporated an additional interacting motif into the PRM-SH3-6His scaffold to study client recruitment through orthogonal binding pairs. The SpyTag peptide, which covalently binds SpyCatcher through an iso-peptide bond, can efficiently drive ADH following the previous recombinant AKR client (Figure 1B,E,F).

Next, the SpyTag-ADH/SpyCatcher-AKR-PRM-SH3-6His (SAAS) phase behavior in vitro was investigated. First, the SAAS protein was self-crosslinking at 80 rpm for one hour at 0 °C. Subsequently, it immediately became turbid when mixed with a droplet formation buffer (5% polyethylene glycol 2000). The turbidity (OD_{350}) increased from 0.173 ± 0.011 (2×10^{-6} M) to 1.99 ± 0.02 (60×10^{-6} M) while increasing the SAAS protein concentration and adding Zn^{2+} in a metal concentration-dependent manner (Figure 2E and Table S6, Supporting Information). Phase separation into droplets occurred in the presence of Zn^{2+} (Figure 2D). After adding biological orthogonal pairs and ordered cross-linking, the resulting phase separation effect was more intense, the confocal fluorescence intensity more pronounced (Figure 2H), and the rate of fluorescence bleaching recovery is also accelerated (Figure 2I). Protein phase separation cannot occur to sole SpyTag-ADH to form droplets. However, droplets can form when it binds to SpyCatcher-AKR-PRM-SH3-6His under the regulation of Zn^{2+} and SpyCatcher/SpyTag bioorthogonal linking. Thus, fluorescence microscopy analysis shows that the colocalized GFP-fused SpyTag-ADH and mCherry-fused SpyCatcher-AKR-PRM-SH3-6His appear yellow fluorescence under both channels simultaneously. The "CFI" and "MFI" refer to the colocalized and total merged fluorescence intensity of GFP and mCherry, respectively (Figure 2H). Recruitment of SpyTag-ADH to the SpyCatcher-AKR-PRM-SH3-6His droplet was shown to be highly precise and effectively combined. The structural domain of Spycatcher-AKR, AKR protein is rich in hydrophobic and polar amino acid residues that order the interactions between PRM-SH3 proteins. Therefore, Spycatcher-AKR, AKR was doped into PRM-SH3-6His to generate recombinant Spycatcher-AKR-PRM-SH3-6His, AKR-PRM-SH3-6His which in turn affects the rigidity of the droplets. The internal fluorescence of PRM-SH3-6His droplets was restored after photobleaching (FRAP) to ≈60%.[22] However, the internal fluorescence of Spycatcher-AKR-PRM-SH3-6His and AKR-PRM-SH3-6His recovered droplets was reduced by 40% (Figure 2I) and 50% (Figure 2G), respectively, compared with PRM-SH3-6His. This result suggests that Spycatcher-AKR, AKR increased the rigidity of the droplets in vitro.[25]

2.3. In Situ Generation and Characterization of Zeolitic Imidazolate Framework-8 (ZIF-8) Encapsulating a Dual Enzyme Cascade System

Histidine-rich proteins can facilitate the formation of prenucleation clusters[17] and the subsequent formation of MOFs around proteins by coordinating with metal ions such as Zn^{2+}[22] to enrich themselves.[42] Addition of Zn^{2+} ions followed by 2-methylimidazole generates prenucleation clusters[20] that form ZIF-8[17] around the recombinant AKR and ADH. ZIF-8 preserves the activity and enhances the stability of encapsulated enzymes[20] (Figure S7 and Table S8, Supporting Information). This dual enzyme system is utilized to catalyze the enzyme cascade reaction shown in **Figure 3A**. In the catalytic reaction, we chose L-clorprenaline and thiophene-benzimidazole intermediate, (S)−1-(2-chlorophenyl) ethanol, as a model product. Phase separation was achieved using AKR-PRM-SH3-6His and 6His-SH3-PRM-ADH, and then embedded in ZIF-8 for just disordered immobilization (DIAA@ZIF-8).

When SpyTag is fused to ADH to obtain SpyTag-ADH, spontaneous cross-linking and covalent assembly of SpyTag-ADH and SpyCatcher-AKR-PRM-SH3-6His produces an ordered dual enzyme system. Subsequent addition of Zn^{2+} ions induced phase separation and embedded SpyTag-ADH and SpyCatcher-AKR-PRM-SH3-6His in ZIF-8 to achieve ordered immobilization (OIAA@ZIF-8). In contrast, nonphase separation-driven embedding of wild AKR and ADH enzymes embedded in ZIF-8 for random immobilization (RIAA@ZIF-8). During the formation of the ZIF-8, when a high concentration of zinc acetate solution, e.g., 40×10^{-3} M, was added to the 30×10^{-6} M AKR-ADH protein, precipitation of the protein was observed to give a flocculent structure. Therefore, we added a 400×10^{-6} M zinc acetate solution in subsequent experiments and observed a phase transition before adding the zinc acetate and dimethylimidazole solutions several times, supplementing with 40×10^{-3} M zinc acetate and 640×10^{-3} M dimethylimidazole.

The results of the scanning electron microscopy (SEM) image (Figure 3B) indicate that ZIF-8 forms a rhombic dodecahedral structure[16] with an average diameter of 100–200 nm. Histidine-rich protein accelerates the biomineralization of zeolitic imidazolate frameworks, promoting the encapsulation of proteins by ZIF-8.[42] The RIAA@ZIF-8, DIAA@ZIF-8, and OIAA@ZIF-8 form a rhombic dodecahedral structure and exhibit an average diameter of 500–600 nm. These results are consistent with the transmission electron microscopy (TEM) characterization (Figure 3C). When encapsulating proteins with six histidines enriching Zn^{2+}, which can promote the formation of prenucleation clusters, ZIF-8 can subsequently form around the proteins. This may increase the size of ZIF-8 compared with that containing no proteins.[42] The ZIF-8 structure can be hydrolyzed by 0.1 M PBS[43] at pH 5 with 1×10^{-3} M HCl[42] (Figure S8, Supporting Information) at 37 °C for 1 h. The ZIF-8 lacking the enzymes and ZIF-8 with encapsulated enzymes showed overlapping X-ray diffraction (XRD) patterns, indicating that both products had crystalline structures (Figure 3D).

The ZIF-8 exhibited a similar XRD pattern to the consistent pattern provided in the previous report,[44] indicating successful synthesis of ZIF-8. There were almost no discernible differences between the OIAA@ZIF-8 and ZIF-8 patterns, except for variations in peak intensities, and no SpyTag-ADH/SpyCatcher-AKR-PRM-SH3-6His (SAAS) diffraction peak was detected. This may be due to the strong interactions between SAAS and ZIF-8 in the synthesized OIAA@ZIF-8. The presence of characteristic peaks in the spectrum of OIAA@ZIF-8 indicated the successful synthesis of OIAA@ZIF-8. Additionally, the formation of DIAA@ZIF-8 and OIAA@ZIF-8 was confirmed by Fourier transform infrared spectroscopy (FTIR) (Figure 3E,G). The FTIR spectra of DIAA@ZIF-8 and OIAA@ZIF-8 exhibit similar trends and differ from that of ZIF-8. The ZIF-8 crystals exhibited

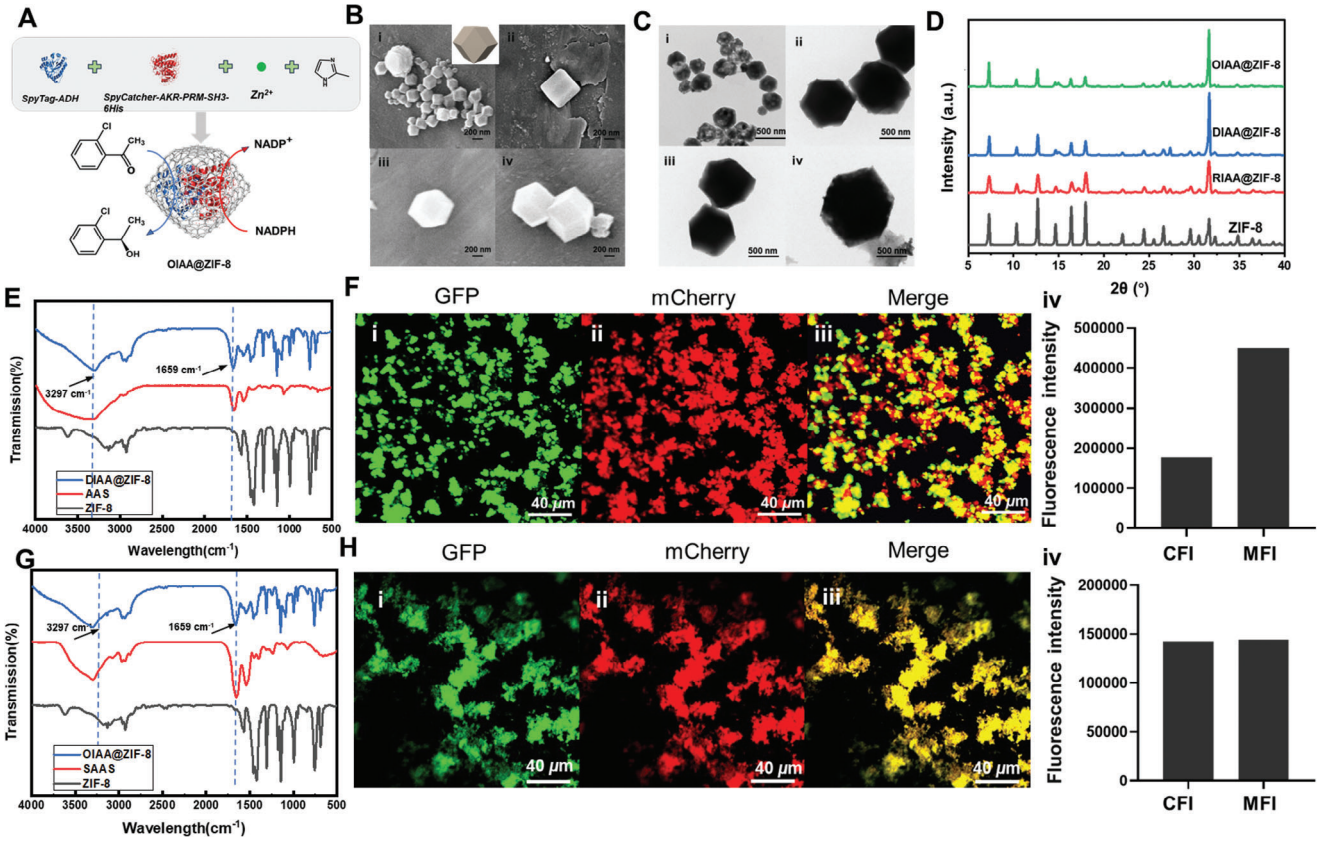

Figure 3. Encapsulation and characterization of AKR/ADH in ZIF-8 by combining bioorthological ligation and protein phase separation. A) Schematic diagram of ZIF-8 embedded AKR-ADH catalyzed reaction. B) SEM image of ZIF-8. Scale bars: 200 nm. i: ZIF-8; ii: RIAA@ZIF-8, iii: DIAA@ZIF-8, iv: OIAA@ZIF-8. C)TEM image of ZIF-8. Scale bars: 500 nm. i: ZIF-8; ii: RIAA@ZIF-8; iii: DIAA@ZIF-8; iv: OIAA@ZIF-8. D) XRD patterns of ZIF-8. E) The FTIR characterization of DIAA@ZIF-8. F) CLSM images of the GFP-fused 6His-SH3-PRM-ADH and mCherry-fused AKR-PRM-SH3-6His-loaded ZIF-8 (DIAA@ZIF-8): excitation of the DIAA@ZIF-8 at 488 nm and monitoring the fluorescence of the GFP-fused 6His-SH3-PRM-ADH at 507 nm; excitation of the DIAA@ZIF-8 at 588 nm and monitoring the fluorescence of the mCherry-fused AKR-PRM-SH3-6His at 610 nm CLSM images of ZIF-8 at 40×10^{-6} M protein are shown in the right. Scale bars: 40×10^{-6} M. Histogram of DIAA@ZIF-8 fluorescence intensity analysis. Confocal is the area of confocal fluorescence intensity in the merge plot, and the total is the area of total fluorescence intensity in the merge plot. G) The FTIR characterization of OIAA@ZIF-8. H) CLSM images of the GFP-fused SpyTag-ADH and mCherry-fused SpyCatcher-AKR-PRM-SH3-6His-loaded ZIF-8 (OIAA@ZIF-8): excitation of the OIAA@ZIF-8 at 488 nm and monitoring the fluorescence of the GFP-fused SpyTag-ADH at 507 nm; excitation of the OIAA@ZIF-8 at 588 nm and monitoring the fluorescence of the mCherry-fused SpyCatcher-AKR-PRM-SH3-6His at 610 nm. CLSM images of OIAA@ZIF-8 at 40×10^{-6} M protein are shown on the right. Scale bars: 40×10^{-6} M. Histogram of OIAA@ZIF-8 fluorescence intensity analysis. The "CFI" and "MFI" refer to the co-localized and total merged fluorescence intensity of GFP and mCherry, respectively.

characteristic peaks at 753 cm^{-1} and 692 cm^{-1} attributed to the vibrations of Zn—O and Zn—N.[45] DIAA@ZIF-8 and OIAA@ZIF-8 underwent disordered and ordered coimmobilization, respectively. The stretching vibrations of carboxylate groups, —OH, and C—O were observed at 3297 cm^{-1} and 1659 cm^{-1}, which are consistent with 6His-SH3-PRM-ADH/AKR-PRM-SH3-6His (AAS) and SAAS.[33] Meanwhile, the peaks at 2927^{-1}, 1593^{-1}, and 1174 cm^{-1} found in the spectrum of ZIF-8 were attributed to the stretching vibrations of C—H, C═N, and C—N, respectively. The presence of characteristic peaks in the spectrum of DIAA@ZIF-8 and OIAA@ZIF-8 indicated the successful synthesis of these materials.[46]

This was further confirmed by fluorescence confocal microscopy imaging of the mCherry-fused AKR and GFP-fused ADH incorporated in the ZIF-8, which demonstrated the confinement of the two enzymes within the ZIF-8. Figure 3F shows the fluorescence properties of the loaded enzymes and merged images of DIAA@ZIF-8. Excitation of the DIAA@ZIF-8 at 488 nm yielded the green fluorescence of the fused protein of 6His-SH3-PRM-ADH with GFP observed. Excitation of the DIAA@ZIF-8 at 588 nm yielded red fluorescence of AKR-PRM-SH3-6His fused with mCherry. The merged image indicates that the two enzymes were encapsulated within the ZIF-8 carriers rather than being attached to the surface. Fluorescence confocal microscopy images of the OIAA@ZIF-8 carrying the different fluorophores are displayed in Figure 3H together with merged images. The overlay of the two fluorescent colors and the merged image confirms the internalization of both enzymes in the ZIF-8. Excitation of the OIAA@ZIF-8 at 488 nm yielded the green fluorescence characteristic of the fusion of SpyTag-ADH with GFP. Excitation of the OIAA@ZIF-8 at 588 nm, in contrast, afforded the red fluorescence of SpyCatcher-AKR-PRM-SH3-6His fused with mCherry. The merged images indicate that the two enzymes are colocalized and embedded in the ZIF-8. The unified yellow of the sample in

Table 1. Apparent kinetic analysis of immobilized enzymes preparations.

Immobilization manner	K_m [× 10^{-3} M]	K_{cat} [s^{-1}]	K_{cat}/K_m
OIAA@ZIF-8	0.468 ± 0.062	0.757 ± 0.022	1.617
DIAA@ZIF-8	0.677 ± 0.082	0.575 ± 0.021	0.849
RIAA@ZIF-8	0.493 ± 0.062	0.344 ± 0.016	0.698

Figure 3H shows that the SpyCatcher-AKR-PRM-SH3-6His and SpyTag-ADH are colocalized in an orderly fashion and the ratio of their molar amounts is 1:1. This demonstrates that they can bind together through bioorthogonal chemistry for cascade biocatalysis. However, if the binding is not through bioorthogonal chemical linking orderly localization can't be ensured, as presented in Figure 3F, separate red and green fluorescence can be seen in addition to the yellow fluorescence of the two channels combined.

Independent assays revealed that AKR or ADH encapsulated in the ZIF-8 retained over 70% of the enzyme activity observed before encapsulation (Table S7, Supporting Information). Regeneration of NADPH cofactor with isopropanol exhibited a reductive activity of 0.932 ± 0.17 U mg^{-1} with OIAA@ZIF-8 and 0.538±0.1 U mg^{-1} with DIAA@ZIF-8. The oxidative activities of OIAA@ZIF-8 and DIAA@ZIF-8 using dihydro-4,4-dimethyl-2,3-furandione (5 mg mL^{-1}) as substrate, were 0.66 ± 0.1 U mg^{-1} and 0.65 ± 0.07 U mg^{-1}, respectively (Table S7, Supporting Information). The loadings of OIAA@ZIF-8 were 500 μg mg^{-1} (for details see Table S8, Supporting Information). Kinetic properties of the dual enzyme preparations, such as DIAA@ZIF-8, OIAA@ZIF-8, and RIAA@ZIF-8, were examined and the extent of the reaction was monitored by detecting the change in UV absorbance value at 340 nm.[33] Substrate concentrations ranging from 0.1 × 10^{-3} to 16 × 10^{-3} M were used and curves were fitted to the reaction rate versus substrate concentration (Figure S9, Supporting Information). OIAA@ZIF-8 exhibits a lower K_m value and higher catalytic efficiency compared to RIAA@ZIF-8, with a K_{cat}/K_m value 2.29 times higher (**Table 1**).

2.4. Enantioselective Biocatalytic Synthesis of Alcohol Using a Dual Enzyme Cascade System Encapsulated in Zeolitic Imidazolate Framework-8 (ZIF-8)

Figure 4A demonstrates that in the catalytic synthesis of (S)-1-(2-chlorophenyl) ethanol, orderly OIAA@ZIF-8 is more efficient than those of DIAA@ZIF-8 and RIAA@ZIF-8. In the HPLC spectrum determination of the reaction solution, there was no obvious peak of (R)−1-(2-chlorophenyl) ethanol, and the enantiomeric excess (ee) value is >99.99%. After 7 h, the yields of the substrate o-chloroacetophenone to (S)-1,2(chlorophenyl)ethanol are 92.4%, 89.6%, and 78.5%, respectively, when OIAA@ZIF-8, DIAA@ZIF-8, and RIAA@ZIF-8 were used. The OIAA@ZIF-8 allows closer proximity between AKR and ADH in the cascade reaction, facilitating more convenient substrate circulation (Figure S10, Supporting Information)

In the SAAS cascade catalytic system, precise colocalization using bioorthogonal chemical linking achieves the desired proximity of the cascade enzymes and the resulting substrate channeling effects. This facilitates exchange of intermediates between active sites and minimizes the loss of unstable intermediates and cofactors. Both OIAA@ZIF-8 and DIAA@ZIF-8 demonstrated higher catalytic activity and selectivity at optimal substrate concentrations compared to RIAA@ZIF-8, suggesting the potential of bioorthogonal chemistry and biological phase transitions for in situ generation of ZIF-8 containing enzymes. The OIAA@ZIF-8 retained its initial 91.1% conversion after 6 cycles of 48 h. Similarly, DIAA@ZIF-8 and RIAA@ZIF-8 maintained initial conversions of 75%, and 72.9%, respectively. Furthermore, the enantiomeric excess (ee) value exceeded 99.99% in each cycle (Figure 4B). We attribute the stable catalytic properties of the enzyme preparations to their confinement in ZIF-8, which can mimic macromolecular crowding observed in the cell.[47–49]

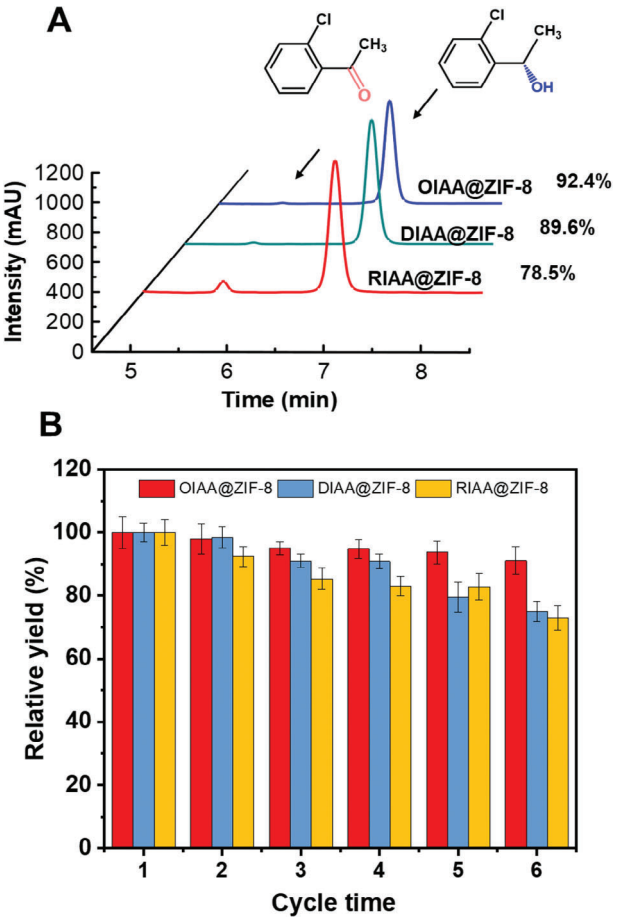

Figure 4. A) HPLC analysis of the product catalyzed by OIAA@ZIF-8, DIAA@ZIF-8, and RIAA@ZIF-8. HPLC analysis of the catalytic synthesis of (S)-1-(2-chlorophenyl) ethanol (retention time of (S)-1-(2-chlorophenyl) ethanol was 6.8 min, and the retention time of the substrate o-chloroacetophenone was 5.54 min). B) Cyclic stability of OIAA@ZIF-8, DIAA@ZIF-8, and RIAA@ZIF-8.

3. Conclusion

Here, we present a new and straightforward approach to in situ generation of ZIF-8 containing spatially aligned dual enzymes using a combination of protein phase separation and bioorthogonal self-crosslinking. Zn^{2+}-driven enzyme phase separation enriched the target enzymes and formed prenucleation clusters,

thus facilitating the generation of ZIF-8 containing the cascade biocatalysis system. The porous structure in ZIF-8 facilitates the diffusion of regenerated NADPH to enable efficient cascade catalysis and acceleration of the reaction. The catalytic synthesis of (S)-1-(2-chlorophenyl) ethanol using OIAA@ZIF-8 maintained high activity and stability after multiple cycles.

This biomimetic mineralization depending on LLPS is an effective methodology for rapidly producing immobilized bioorthogonal multienzyme systems. The resulting multienzyme systems present robust activity through the substrate channeling effect, which makes them suitable for catalyzing the biosynthesis of complex natural bioactive molecules, such as terpenoids. Additionally, the obtained ZIF-8 particles encapsulating multienzymes can be reused and also fulfilled in pipeline flow chemistry. Based on this, they would be widely applied in large-scale synthesis of fine chemicals and pharmaceutical intermediates.[50]

Supporting Information

Supporting Information is available from the Wiley Online Library or from the author.

Acknowledgements

This work was supported by the National Natural Science Foundation of China (22078079, 22378091), the Natural Science Foundation of Zhejiang Province (LY18B060009), the Program for Postgraduates in Innovation Practice and Service for Locality in HZNU (2022), and the University Students' Science and Technology Innovation Activity Program and New Seedling Talent Program of Zhejiang Province (2023R445076).

Conflict of Interest

The authors declare no conflict of interest.

Data Availability Statement

The data that support the findings of this study are available from the corresponding author upon reasonable request.

Keywords

biocatalytic cascades, bioorthogonal chemistry, MOF nanoreactor, protein liquid–liquid phase separation

Received: May 17, 2024
Revised: June 28, 2024
Published online:

[1] A. I. Benítez-Mateos, D. Roura Padrosa, F. Paradisi, *Nat. Chem.* **2022**, *14*, 489.
[2] A. Fryszkowska, O. Alvizo, M. Borra-Garske, K. R. Campos, K. A. Canada, P. N. Devine, D. Duan, J. H. Forstater, S. T. Grosser, H. M. Halsey, G. J. Hughes, J. Jo, L. A. Joyce, J. N. Kolev, J. Liang, K. M. Maloney, B. F. Mann, N. M. Marshall, M. McLaughlin, J. C. Moore, G. S. Murphy, C. C. Nawrat, J. Nazor, S. Novick, N. R. Patel, A. Rodriguez-Granillo, S. A. Robaire, E. C. Sherer, M. D. Truppo, A. M. Whittaker, et al., *Science* **2019**, *366*, 1255.
[3] Y.-Q. Zhang, T.-T. Feng, Y.-F. Cao, X.-Y. Zhang, T. Wang, M. R. Huanca Nina, L.-C. Wang, H.-L. Yu, J.-H. Xu, J. Ge, Y.-P. Bai, *ACS Catal.* **2021**, *11*, 10487.
[4] R. Hao, M. Zhang, D. Tian, F. Lei, Z. Qin, T. Wu, H. Yang, *J. Am. Chem. Soc.* **2023**, *145*, 20319.
[5] N. Miložič, M. Lubej, M. Lakner, P. Žnidaršič-Plazl, I. Plazl, *Chem. Eng. J.* **2017**, *313*, 374.
[6] F. V. Schmidt, L. Schulz, J. Zarzycki, S. Prinz, N. N. Oehlmann, T. J. Erb, J. G. Rebelein, *Nat. Struct. Mol. Biol.* **2023**, *31*, 150.
[7] Y. Wang, M. Liu, Q. Wei, W. Wu, Y. He, J. Gao, R. Zhou, L. Jiang, J. Qu, J. Xia, *Angew. Chem., Int. Ed.* **2022**, *61*, e202203909.
[8] J. M. Sperl, V. Sieber, *ACS Catal.* **2018**, *8*, 2385.
[9] J. Zdarta, A. Kołodziejczak-Radzimska, K. Bachosz, A. Rybarczyk, M. Bilal, H. M. N. Iqbal, B. Buszewski, T. Jesionowski, *Adv. Colloid Interface Sci.* **2023**, *315*, 102889.
[10] J. C. Breger, J. N. Vranish, E. Oh, M. H. Stewart, K. Susumu, G. Lasarte-Aragonés, G. A. Ellis, S. A. Walper, S. A. Díaz, S. L. Hooe, W. P. Klein, M. Thakur, M. G. Ancona, I. L. Medintz, *Nat. Commun.* **2023**, *14*, 1757.
[11] S. S. Nadar, V. K. Rathod, *Biocatal. Agric. Biotechnol.* **2019**, *17*, 470.
[12] K. S. Park, Z. Ni, A. P. Cote, J. Y. Choi, R. Huang, F. J. Uribe-Romo, H. K. Chae, M. O'Keeffe, O. M. Yaghi, *Proc. Natl. Acad. Sci. USA* **2006**, *103*, 10186.
[13] S. Qiao, H. Jin, A. Zuo, Y. Chen, *Acc. Chem. Res.* **2023**, *57*, 93.
[14] H. Groeger, A. Allahverdiyev, J. Yang, J. Stiehm, *Adv. Funct. Mater.* **2024**, 2304794.
[15] A. R. M. Silva, J. Y. N. H. Alexandre, J. E. S. Souza, J. G. Lima Neto, P. G. de Sousa Junior, M. V. P. Rocha, J. C. S. dos Santos, *Molecules* **2022**, *27*, 4529.
[16] E. Astria, M. Thonhofer, R. Ricco, W. Liang, A. Chemelli, A. Tarzia, K. Alt, C. E. Hagemeyer, J. Rattenberger, H. Schroettner, T. Wrodnigg, H. Amenitsch, D. M. Huang, C. J. Doonan, P. Falcaro, *Mater. Horiz.* **2019**, *6*, 969.
[17] G. Chen, S. Huang, X. Kou, S. Wei, S. Huang, S. Jiang, J. Shen, F. Zhu, G. Ouyang, *Angew. Chem., Int. Ed.* **2019**, *58*, 1463.
[18] S. Liang, X. L. Wu, J. Xiong, M. H. Zong, W. Y. Lou, *Coord. Chem. Rev.* **2020**, *406*, 213149.
[19] Y. Cao, X. Li, J. Xiong, L. Wang, L.-T. Yan, J. Ge, *Nanoscale* **2019**, *11*, 22108.
[20] W.-H. Chen, M. Vázquez-González, A. Zoabi, R. Abu-Reziq, I. Willner, *Nat. Catal.* **2018**, *1*, 689.
[21] X. G. Yang, J. R. Zhang, X. K. Tian, J. H. Qin, X. Y. Zhang, L. F. Ma, *Angew. Chem.* **2023**, *135*, e202216699.
[22] K. Hong, D. Song, Y. Jung, *Nat. Commun.* **2020**, *11*, 5554.
[23] T. Piou, L.-C. Campeau, *Nat. Chem.* **2021**, *13*, 1027.
[24] M. Dzuricky, B. A. Rogers, A. Shahid, P. S. Cremer, A. Chilkoti, *Nat. Chem.* **2020**, *12*, 814.
[25] P. Zhou, H. Liu, X. Meng, H. Zuo, M. Qi, L. Guo, C. Gao, W. Song, J. Wu, X. Chen, W. Chen, L. Liu, *Angew. Chem., Int. Ed.* **2023**, *62*, e202215778.
[26] M. Liu, S. He, L. Cheng, J. Qu, J. Xia, *Biomacromolecules* **2020**, *21*, 2391.
[27] P. Li, S. Banjade, H.-C. Cheng, S. Kim, B. Chen, L. Guo, M. Llaguno, J. V. Hollingsworth, D. S. King, S. F. Banani, P. S. Russo, Q.-X. Jiang, B. T. Nixon, M. K. Rosen, *Nature* **2012**, *483*, 336.
[28] B. S. Schuster, E. H. Reed, R. Parthasarathy, C. N. Jahnke, R. M. Caldwell, J. G. Bermudez, H. Ramage, M. C. Good, D. A. Hammer, *Nat. Commun.* **2018**, *9*, 2985.
[29] J. Berry, C. P. Brangwynne, M. Haataja, *Rep. Prog. Phys.* **2018**, *81*, 046601.
[30] W. J. Altenburg, N. A. Yewdall, D. F. M. Vervoort, M. H. M. E. van Stevendaal, A. F. Mason, J. C. M. van Hest, *Nat. Commun.* **2020**, *11*, 6282.

[31] J. Wang, J.-M. Choi, A. S. Holehouse, H. O. Lee, X. Zhang, M. Jahnel, S. Maharana, R. Lemaitre, A. Pozniakovsky, D. Drechsel, I. Poser, R. V. Pappu, S. Alberti, A. A. Hyman, *Cell* **2018**, *174*, 688.
[32] D. Zhu, S. Ao, H. Deng, M. Wang, C. Qin, J. Zhang, Y. Jia, P. Ye, H. Ni, *ACS Appl. Mater. Interfaces* **2019**, *11*, 33581.
[33] L. Qiao, Z. Luo, R. Wang, X. Pei, S. Wu, H. Chen, T. Xie, R. A. Sheldon, A. Wang, *Green Chem.* **2023**, *25*, 7547.
[34] X. Pei, Z. Luo, L. Qiao, Q. Xiao, P. Zhang, A. Wang, R. A. Sheldon, *Chem. Soc. Rev.* **2022**, *51*, 7281.
[35] A. H. Keeble, A. Banerjee, M. P. Ferla, S. C. Reddington, I. N. A. K. Anuar, M. Howarth, *Angew. Chem., Int. Ed.* **2017**, *56*, 16521.
[36] M. Liu, Y. Song, Y. H. P. J. Zhang, C. You, *ChemSusChem* **2023**, *16*, 202202153.
[37] R. Kratzer, J. M. Woodley, B. Nidetzky, *Biotechnol. Adv.* **2015**, *33*, 1641.
[38] T. M. Penning, S. Jonnalagadda, P. C. Trippier, T. L. Rizner, *Pharmacol. Rev.* **2021**, *73*, 1150.
[39] J. Zhu, L. Jiang, *Langmuir* **2022**, *38*, 9043.
[40] X. Jia, L. Lin, S. Xu, L. Li, Z. Wei, C. Yu, F. Niu, *Int. J. Mol. Sci.* **2023**, *24*, 1414.
[41] P. Luan, Y. Li, C. Huang, L. Dong, T. Ma, J. Liu, J. Gao, Y. Liu, Y. Jiang, *ACS Catal.* **2022**, *12*, 7550.
[42] Q. Zheng, J. Sheng, J. Liu, X. Chen, M. Wang, *Biomacromolecules* **2023**, *24*, 5132.
[43] M. d. J. Velásquez-Hernández, R. Ricco, F. Carraro, F. T. Limpoco, M. Linares-Moreau, E. Leitner, H. Wiltsche, J. Rattenberger, H. Schröttner, P. Frühwirt, E. M. Stadler, G. Gescheidt, H. Amenitsch, C. J. Doonan, P. Falcaro, *CrystEngComm* **2019**, *21*, 4538.
[44] P. M. Gurave, B. Nandan, R. K. Srivastava, *J. Membr. Sci.* **2023**, *683*, 121850.
[45] J. Li, L. Li, X. Li, L. Dong, Z. Wang, J. Shen, B. Van der Bruggen, *Desalination* **2023**, *546*, 116184.
[46] X. Pei, Y. Wu, J. Wang, Z. Chen, W. Liu, W. Su, F. Liu, *Nanoscale* **2020**, *12*, 967.
[47] M. Bonucci, T. Shu, L. J. Holt, *Trends Cell Biol.* **2023**, *33*, 924.
[48] H.-X. Zhou, G. Rivas, A. P. Minton, *Annu. Rev. Biophys.* **2008**, *37*, 375.
[49] G. Rivas, A. P. Minton, *Trends Biochem. Sci.* **2016**, *41*, 970.
[50] A. Ledesma-Fernandez, S. Velasco-Lozano, J. Santiago-Arcos, F. Lopez-Gallego, A. L. L. Cortajarena, *Nat. Commun.* **2023**, *14*, 2587.